The role of the amorphous phase in melting of linear UHMW-PE; implications for chain dynamics

2007 J. Phys.: Condens. Matter 19 205122

(http://iopscience.iop.org/0953-8984/19/20/205122)

IOP PUBLISHING JOURNAL OF PHYSICS: CONDENSED MATTER

J. Phys.: Condens. Matter **19** (2007) 205122 (21pp) doi:10.1088/0953-8984/19/20/205122

The role of the amorphous phase in melting of linear UHMW-PE; implications for chain dynamics

Sanjay Rastogi[1,2], **Dirk R Lippits**[1,3], **Günther W H Höhne**[1], **Brahim Mezari**[1] **and Pieter C M M Magusin**[1]

[1] Department of Chemical Engineering and Chemistry/The Dutch Polymer Institute, Eindhoven University of Technology, PO Box 513, 5600MB Eindhoven, The Netherlands
[2] IPTME, Loughborough University, Leicestershire LE11 3TU, UK
[3] DSM Research, PO box 18, 6160 MD, Geleen, The Netherlands

E-mail: s.rastogi@tue.nl and s.rastogi@lboro.ac.uk

Received 14 October 2006
Published 25 April 2007
Online at stacks.iop.org/JPhysCM/19/205122

Abstract

In ultra-high molecular weight polyethylene (UHMW-PE), it is possible to obtain single chain forming single crystals, where chains are adjacently re-entrant. Depending on the heating rate, it is feasible to melt these crystals either by simple consecutive detachment of chain stems from the crystalline substrate or by cluster melting, where several chain stems are involved. The consecutive detachment of chain stems occurs at the melting point predicted from the Gibbs–Thomson equation, whereas the cluster melting at much higher temperatures. Melting by the consecutive detachment of chain stems from the crystal substrate and their diffusion in the melt ultimately result in a new melt state having a heterogeneous distribution of physical entanglements, which invokes differences in local mobility. With combined DSC, rheology and solid-state NMR studies, it is concluded that the disentangled domains present within the entangled matrix possess higher local mobility than the entangled domains, ultimately causing lower elastic modulus. The fraction of the entangled and disentangled domains is maintained at higher temperatures, leading to a thermodynamically non-equilibrium melt state. In contrast, in cluster melting, where several chain stems (initially disentangled) can simultaneously adopt the random coil state, entanglements that are formed are homogeneously distributed in the melt. The paper invokes the influence of the topological differences present in the amorphous phase of the semi-crystalline polymer on the melting kinetics of crystals. The reported findings have implications for the melting behaviour and the resulting melt state of polymers in general.

(Some figures in this article are in colour only in the electronic version)

1. Introduction

In semi-crystalline polymers crystalline regions are linked by amorphous domains. Depending on the crystallization conditions, chain stiffness, and molecular weight a chain may traverse between crystals or fold back within the parent crystal. In this paper, we investigate a well studied flexible polymer—ultra-high molecular weight linear polyethylene of molar mass greater than 10^6 g mol^{-1} (UHMW-PE). Entanglements present in the amorphous phase influence mechanical deformation of the polymer in the solid state, which show a strong dependence on the synthesis conditions [1–3].

Entanglements in the amorphous region can also be controlled by crystallizing the polymer from solution. Below a critical initial concentration the entanglements within the amorphous phase of the resulting material are reduced to such an extent that the solution cast films can be drawn more than 150 times in the solid state [4]. Recently, we demonstrated that careful synthesis with a single site catalyst produces PE with a single chain forming a single crystal. These crystals can be drawn in the solid state more than 150 times [3]. The solid-state drawability is lost once the materials are molten and crystallized subsequently. This loss in drawability is attributed to the formation of entanglements in the amorphous region of the semi-crystalline polymer influencing the chain topology between the crystalline domains. Synthesis with the highly active heterogeneous Ziegler–Natta catalyst yields nascent (entangled) UHMW-PE, which is less drawable in the solid state (seven times), indicating the influence of the synthesis conditions on the topological chain structure in the amorphous region of the semi-crystalline polymers.

The experimental observations are that melting temperatures of the solution, nascent (i.e. directly obtained from synthesis) and melt crystallized samples of the same polymer are distinctly different. For example, on heating at 10 °C min^{-1}, nascent UHMW-PE melts around 141 °C, close to the reported equilibrium melting temperature for polyethylene of 141.5 °C. Such high melting temperature has been a subject of debate. Using electron microscopy and DSC, Engelen *et al* [5] conclusively showed that the nascent crystals are folded chain crystals. Thus the high melting temperature was attributed to fast reorganization, leading to successive thickening prior to melting. However, no experimental evidence of successive thickening was provided. On the contrary, Kurelec *et al* showed that even on annealing close to the melting point for several hours these nascent crystals do not exceed a value of 26 nm [6, 7]. The melting temperature predicted from the Gibbs–Thomson equation for polyethylene [8] ($T_m = 414.2 - 259.7/l$) for a lamella thickness of 26 nm is 131 °C.[4] Furthermore, the high melting temperature of 141 °C is lost on second heating, where a melting temperature of 135 °C [5] is measured. A similar discrepancy is observed between the first and second heating runs of solution crystallized UHMW-PE, where the lamellae double their initial thickness upon annealing below the melting temperature to a maximum of 25 nm [10]. The melting temperature predicted from the Gibbs–Thomson equation for a lamella thickness of 25 nm is also approximately 131 °C, 5 °C lower than the experimentally observed melting point of 136 °C. Furthermore, the high melting temperature of 136 °C is lost on second heating, where a melting temperature of 131 °C is measured, which now coincides with the prediction of the Gibbs–Thomson equation.

The melting aspects involved in nascent, melt- and solution-crystallized polymers cannot be explained by existing thermodynamic concepts alone. In this paper we present an enlarged

[4] The authors are aware that, depending on the experimental methods used, different numerical Gibbs–Thomson equations exist; see [9]. A difference arises because of different surface free energy values, resulting in a somewhat different melting temperature of 136 °C for a crystal thickness of 25 nm. But such discrepancies in the calculated melting temperatures have no implications for our experimental findings.

Table 1. Molecular properties and synthesis temperature conditions of the UHMW-PE samples.

	M_w (g mol^{-1})	M_w/M_n	Melting peak on first heating (°C)	Draw ratio at 120 °C
Nascent, entangled	4.5×10^6	8	141	7
Nascent, disentangled	3.6×10^6	3.0	141	>150
Solution crystallized	4.5×10^6	8	136	>150
Melt crystallized	4.5×10^6	8	135	7

investigation in the melting behaviour of these polymers [11]. We correlate the time, as well as the temperature, required for melting to the chain topology in the amorphous phase. The introduced kinetic aspect of melting is probed by different experimental techniques; differential scanning calorimetry (DSC), temperature modulated differential scanning calorimetry (TM-DSC), rheometry and solid-state ^{1}H NMR relaxometry. The key observation in our present study is that at sufficiently low heating rates disentangled nascent polyethylene melts at lower temperatures than observed in normal heating runs. The lowest temperature where melting is observed corresponds to the value predicted by the Gibbs–Thomson equation. This points to the effect of topological constraints in the amorphous domains on the melting of the crystalline regions in the semi-crystalline polymer. Reported findings in this paper should hold for melting of polymers in general.

2. Experimental section

2.1. Materials

To correlate the melting behaviour of UHMW-PE to the chain topology, four different samples were used as described in table 1. The nascent grades differ in synthesis conditions and catalyst type. The nascent entangled sample is a commercial grade of Montell (1900CM) synthesized with a heterogeneous Ziegler–Natta catalyst. The nascent disentangled grade is provided by DSM (The Netherlands), synthesized at temperatures below the dissolution temperature using a homogeneous metallocene catalyst.

The solution crystallized samples were obtained with the entangled nascent UHMW-PE on crystallization from solution (for example 1 wt% of UHMW-PE in decalin). Crystals thus obtained are disentangled and have been investigated in detail before [10]. The melt crystallized samples were obtained by cooling the entangled melt with 10 °C min^{-1}.

Tensile testing was used to investigate the drawability of the materials. In our definition drawable materials (>150 times) are 'disentangled' and un-drawable (<7) materials are 'entangled'.

2.2. Experimental techniques

2.2.1. Differential scanning calorimetry (DSC) has been performed using a standard Perkin-Elmer DSC-7. Samples of 0.7–2.0 mg mass are weighed with a precision balance and encapsulated in standard (crimped) aluminium pans of known mass. An identical empty pan is used as a reference. Nitrogen is purged at a rate of 25 ml min^{-1}. DSC is calibrated using indium and tin.

2.2.2. Tensile testing. For draw ratio determination dumb-bell-shaped samples having a gauge length of 10 mm and a width of 0.5 mm are used. Samples are drawn in solid state at a crosshead speed of 50 mm min^{-1} at 125 °C. The draw ratio is determined by measuring the separation of the ink marks prior to and after the deformation.

2.2.3. Rheometry. Oscillatory shear measurements in the linear viscoelastic region are performed using an advanced rheometrics expansion system (ARES). Measurements are carried out using parallel plate geometry (8 mm diameter) at a constant temperature of 134 °C below the peak melting point in the nitrogen atmosphere. Elastic modulus is followed as a function of time at a constant frequency of 10 rad s^{-1}, at a constant strain of 0.5%. Before measurements the samples are heated with 1 °C min^{-1} from 120 to 134 °C. The pre-melting of the polymer is used to achieve good adhesion between the sample and the plates. To monitor any slippage between the plates and the polymer an oscilloscope is attached to follow any changes in the applied strain.

2.2.4. Solid-state ^1H NMR. NMR experiments are carried out without sample rotation on a Bruker DMX spectrometer operating at a ^{1}H NMR frequency of 500 MHz and equipped with a special (7 mm MAS) probehead that resists temperatures above 150 °C. The transverse relaxation time T_2 is measured using a two pulse sequence 90°-τ-180°-τ-aq with a variable τ time starting from $\tau = 2$ μs. The 90° pulse length was 5 μs and the repetition time was 3 s, which proved long enough for quantitative measurements. The relaxation decay is characterized by 60 data points at properly selected echo times. This pulse sequence is chosen because it offers the possibility to both qualitatively as well as quantitatively analyse relaxation of the amorphous and crystalline components. Temperature calibration is carried out by monitoring peak separation in the ^{1}H NMR spectrum of glycol and the melting-induced ^{1}H NMR line-narrowing of a series of compounds also employed as DSC reference materials. ^{1}H NMR spin–spin relaxation decays are obtained from the total integral of the spectra after Fourier transformation, phase and baseline correction. The relaxation decay is analysed by a non-linear least square fitting. The relaxation times are determined by fitting the relaxation data with a sum of two or three exponentials. From the determined relaxation times below the melting point appropriate τ-delay times are chosen for real-time monitoring of the T_2 relaxation by 12 data points. In this way it is possible to follow the changes in the sample with 5 min intervals.

2.2.5. Temperature modulated differential scanning calorimetry (TM-DSC). Has been performed using a standard Perkin Elmer DSC-7 apparatus modified for temperature modulation [12]. For the TM-DSC measurements an underlying heating rate of 0.5 °C min^{-1} is used, which is low enough to ensure good linearity and stability during measurements. Time dependent temperature modulated measurements are performed in quasi-isothermal mode at different temperatures (110, 120, 130, 135, 136, 137 and 138 °C) at a frequency of 12.5 MHz. The temperature amplitude T_A of 53 mK is kept low enough to ensure a linear response. Before evaluation, the empty pan run (taking the same measuring parameters and phase position) is subtracted from the curve of the sample to reduce surroundings and apparatus influences. The measured (modulated) heat flow rate signal $\Phi(T, t)$ consists of two parts: the underlying part $\Phi_u(t)$ and the periodic part $\Phi_{per}(T, t)$. Gliding integration over one period provides the underlying part $\Phi_u(t)$, which, when subtracted from the total measured signal, yields the periodic part $\Phi_{per}(T, t)$. The apparent heat capacity is calculated using a mathematical procedure described in [13].

3. Results and discussion

3.1. First melting point of nascent UHMW-PE

Figure 1 shows a standard DSC run on the entangled and disentangled nascent UHMW-PE. The observations are that, independent of the synthesis route, no differences in the melting peak,

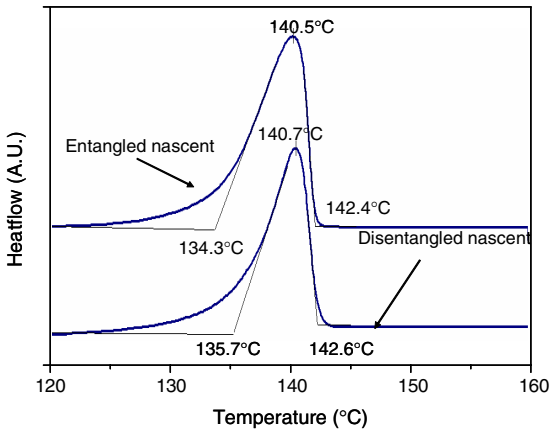

Figure 1. DSC curves obtained on heating the nascent entangled and the nascent disentangled samples at 10 °C min^{-1}. Independent of the synthesis route the polymer melts at 140.5 °C, close to the equilibrium melting point of the linear polyethylene.

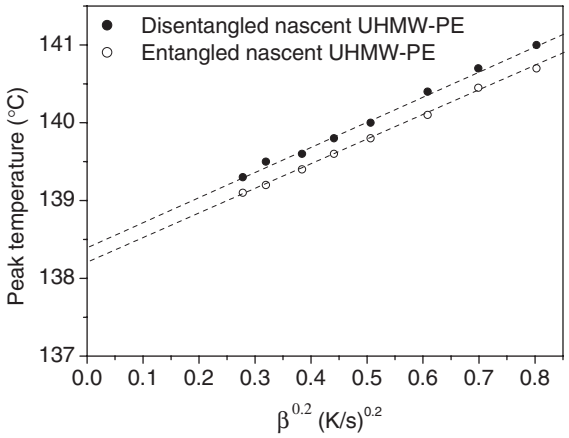

Figure 2. Measured melting peak temperatures for the entangled and the disentangled nascent ultra-high molecular weight polyethylenes (UHMW-PEs) at different heating rates (β).

onset and end temperatures exist, though the polydispersity and the topological constraints (estimated by differences in the drawability of the two samples in the solid state [1, 2]) provided during synthesis of the two samples are different. The observed high melting point of 141 °C of the nascent powders is 5–6 °C higher than for melt-crystallized UHMW-PE [14]. In the heating rate region of 20–0.1 °C min^{-1}, a non-linear relationship between the peak temperature and the heating rate of entangled and disentangled nascent UHMW-PE polymer is observed. However, the melting temperature, plotted against the heating rate to the power 0.2, shows a linear relationship (figure 2). Similar observations are reported by Toda *et al* [15]; however, unlike Toda *et al* no instrumental corrections are applied in the measurements reported here. The 'true' melting temperature is determined by extrapolation to zero heating rate. The shift in the observed melting temperature at non-zero heating rates is attributed to 'superheating'. This superheating is caused (i) by thermal inertia (the transport of heat from the heater to the sample) and (ii) by time dependence of the melting process. Adopting this existing knowledge,

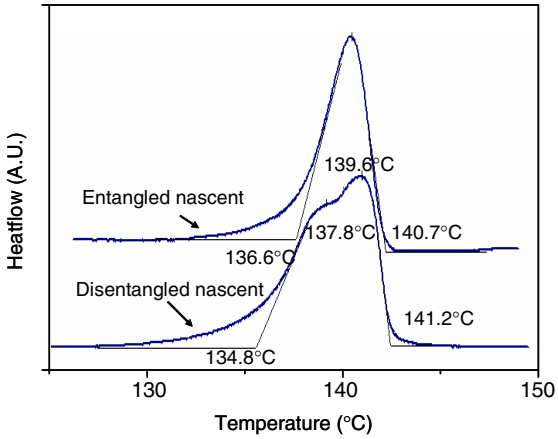

Figure 3. Heating of the nascent entangled UHMW-PE and the nascent disentangled UHMW-PE at 0.1 °C min^{-1}. On slow heating, a second melting peak appears in the disentangled nascent sample.

the extrapolated, 'true' melting temperature for these nascent polymers is 138.4 and 138.2 °C for the disentangled and entangled samples, respectively (figure 2). With the mentioned Gibbs–Thomson equation this melting temperature corresponds to a crystal thickness of approximately 100 nm.[5] However, the experimental observations are that the crystals do not thicken more than a maximum of 26 nm [6, 7] even when the sample is left to anneal for several hours at 120 °C.

3.2. Melting kinetics in UHMW-PE probed by DSC

Figure 3 shows that on decreasing the heating rate to 0.1 °C min^{-1} on the first heating of the disentangled UHMW-PE a second peak at lower temperature appears, whereas in the entangled UHMW-PE a single peak is observed. These results suggest that when given sufficient time an additional melting can occur at lower temperatures. To get more insight into this melting mechanism, annealing experiments below the 'true' melting point of 138.4 °C (determined from figure 2) are performed.

The annealing experiments are performed in the region from 132 to 138 °C. After annealing at the requisite temperature, the sample is cooled to room temperature and reheated (at 10 °C min^{-1}) to 150 °C. On re-heating, two melting peaks at 135 and 141 °C are observed (figure 4). The peak at 135 °C is associated with the melting of the sample which was molten and re-crystallized during cooling from the annealing temperature and the second peak at 141 °C to the crystal domains in the initial nascent state. The ratio between the areas of the two peaks changes with the annealing time at the given annealing temperature. As the peak area is proportional to the amount of the respective crystals, the ratio between the areas is also a measure for the ratio between the amounts of crystals which are re-crystallized and are in the initial nascent state.

The annealing experiments with the disentangled nascent UHMW-PE above 135.5 °C show an exponential decrease of the high temperature peak area with one characteristic time constant (figure 5(a)), whereas at annealing temperatures below 135.5 °C more than one time constant is found (figure 5(b)), suggesting two different melt processes. Similar experiments

[5] From Cho *et al* [16] the calculated crystal thickness for the melting temperature of 138.4 °C is 47 nm; this is also larger than the measured thickness.

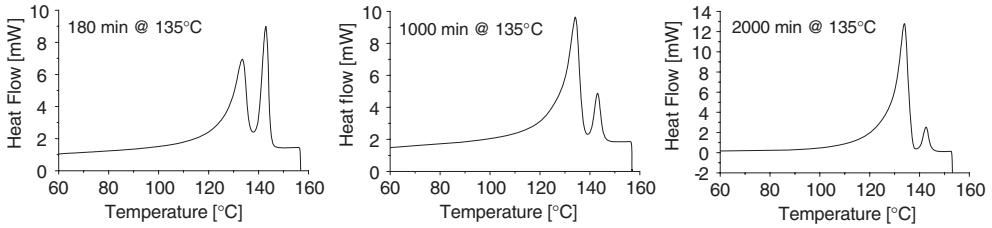

Figure 4. Heating run of the disentangled UHMW-PE, after annealing at 135 °C for different annealing times. The annealing times are mentioned in the corresponding figures. The first peak at 133 °C corresponds to melting of the crystals which crystallized from the melt obtained on annealing. The second peak at 141 °C corresponds to the nascent crystals. The high temperature melting peak disappears on annealing the sample at 135 °C (reproduced from [11]).

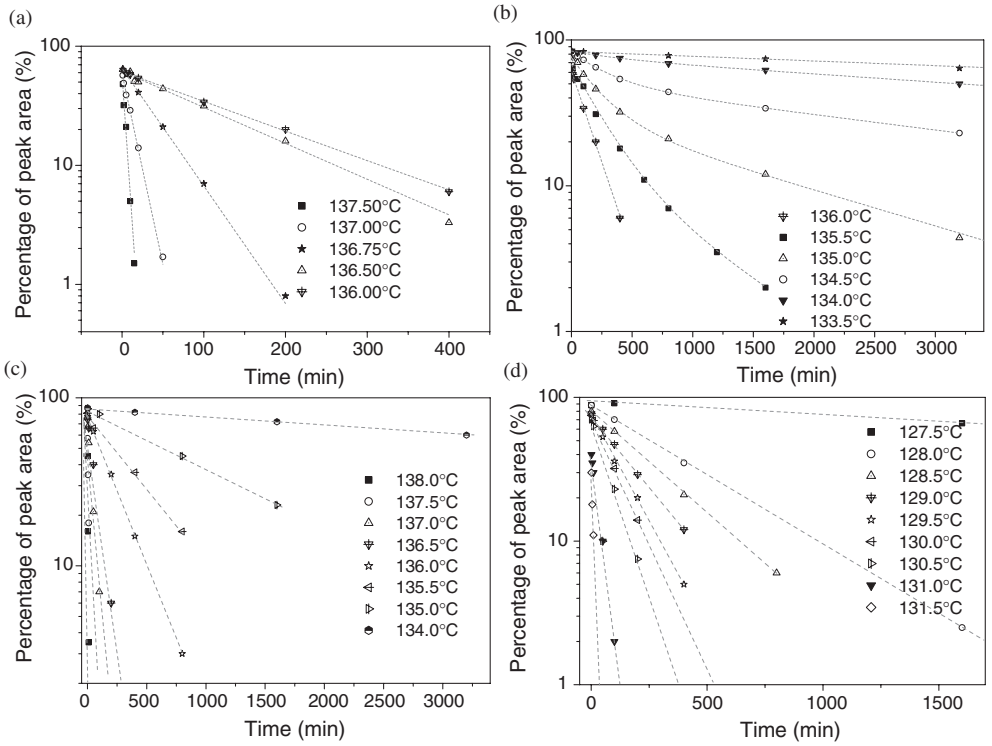

Figure 5. The decrease in the relative area of the high temperature melting peak of the disentangled ((a) and (b)) and entangled (c) nascent UHMW-PEs and solution crystallized samples (d), for different annealing times at different annealing temperatures (reproduced from [11]).

performed on the nascent entangled UHMW-PE and solution crystallized UHMW-PE show one single exponential decrease of the peak area (figures 5(c) and (d), respectively).

From figure 5, it is possible to determine the enthalpic relaxation times for the different melt processes of the different samples. With the time law of Debye (Arrhenius) type for the fusion process in question, the enthalpy change reads

$$H(T,t) = H_0(T)\mathrm{e}^{-t/\tau(T)} \tag{1}$$

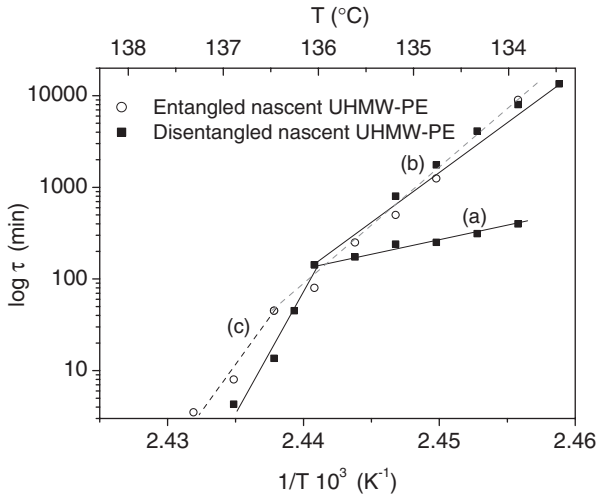

Figure 6. Arrhenius plot of the time constants determined from the slopes of the curves in figures 5(a)–(c) for the entangled and disentangled nascent UHMW-PEs. The activation energies of the three different enthalpic processes are realized from the three different slopes of the curves in the figure (reproduced from [11]).

where the time constant (τ) can be related to an activation energy (E_A) by

$$\tau = \tau_0 e^{E_A/RT}. \tag{2}$$

Figure 6 summarizes the relaxation times determined from the slopes in figure 5. Closed symbols represent the relaxation times for the disentangled nascent UHMW-PE sample. Open symbols in the figure represent the relaxation times for the nascent entangled sample. For the disentangled sample only one single relaxation time exists above 135.5 °C, whereas below this temperature two relaxation times are observed. Unlike the disentangled sample, the entangled polymer shows only one relaxation time over the whole temperature range of 133–138 °C.

Plotting $\log \tau$ versus $1/T$ (figure 6), three different slopes of the relaxation times are observed, indicating the involvement of three different activation energies in the two different temperature regions as shown in table 2. The activation energies vary from $5.0 \pm 1.0 \times 10^3$ kJ mol^{-1} (from slope (c)) for temperatures above 136 °C to $2.1 \pm 0.2 \times 10^3$ kJ mol^{-1} (from slope (b)) and $0.6 \pm 0.05 \times 10^3$ kJ mol^{-1} (from slope (a)) for temperatures below 136 °C, respectively.

The three activation energies suggest the involvement of three different melting processes in the disentangled nascent UHMW-PE. The measured activation energies can be assigned to detachment/removal of chain stem(s) from the crystal, followed by the diffusion of the detached chain into the melt [17]. The measured lowest activation energy of $0.6 \pm 0.05 \times 10^3$ kJ mol^{-1} (a) can be assigned to a cooperative detachment of only a couple of chain stems from the crystal surface and their diffusion. The activation energy of $2.1 \pm 0.2 \times 10^3$ kJ mol^{-1} (b) then refers to the simultaneous detachment of a larger number of stems from the crystalline substrate and their diffusion and finally that of $5.0 \pm 1.0 \times 10^3$ kJ mol^{-1} (c) refers to the cooperative breakdown of larger parts of the crystal lattice. The low activation energies determined from the slopes (a) and (b) suggest the involvement of a new melting behaviour, whereas the slope (c) refers to the conventional melting at higher temperatures.

The activation energy of 0.6×10^3 kJ mol^{-1} (a) can be assigned to the detachment of a chain segment of ∼28 nm (this has been calculated considering the activation energy for detachment

Table 2. Activation energy determined from the Arrhenius plot shown in figures 6 and 7.

	Activation energy[a] ($\times 10^3$ kJ mol^{-1})	Number of CH_2 units involved	Chain length involved (nm)	Lamellae thickness (nm) prior to melt	Stems involved
Nascent entangled	4.3 ± 1.0 (c)	1600 ± 370	202 ± 50	26 [6, 7]	6–10
	2.4 ± 0.2 (b)	900 ± 90	110 ± 10	26 [6, 7]	4–5
Nascent disentangled	5.0 ± 1.0 (c)	1850 ± 370	235 ± 50	26 [6, 7]	7–11
	2.1 ± 0.2 (b)	780 ± 50	99 ± 7	26 [6, 7]	4
	0.6 ± 0.05 (a)	220 ± 20	28 ± 2	26 [6, 7]	1
Solution crystallized	4.2 ± 1.0 (c)	1560 ± 370	197 ± 50	25 [10]	6–10
	0.7 ± 0.05 (a)	250 ± 20	32 ± 2	25 [10]	1

[a] (a), (b) and (c) refer to the three slopes determined from figures 6 and 7. Activation energies in the table are determined from slopes in the figures.

of one CH_2 group and its diffusion into the melt, 2.7 kJ mol^{-1}, and the C–C distance in the orthorhombic lattice along the *c*-axis, 0.127 nm)[6]. Such a segment equals roughly one chain (stem) at the lateral surface of the lamellar crystal. The higher activation energy of $2.1 \pm 0.2 \times 10^3$ kJ mol^{-1} (b) then refers to the simultaneous detachment of three or four stems from the crystalline substrate and their cooperative diffusion and that of $5.0 \pm 1.0 \times 10^3$ kJ mol^{-1} (c) refers to the breakdown of the crystal by simultaneous randomization of at least seven or eight stems.

In contrast to the disentangled polymer, the entangled polymer exhibits the absence of the process leading to the slope of (a), suggesting the absence of melting with consecutive detachment of single chain stems from the crystalline substrate. Apparently this process is not possible due to constraints in the amorphous layers. The slopes of (b) and (c) of the entangled and the disentangled samples are similar, which indicates that melting of the entangled sample occurs in clusters of several chain stems. Such a melting process further confirms the presence of topological constraints in the nascent entangled UHMW-PE compared to the disentangled UHMW-PE.

Figure 7 shows the time constants of the enthalpic relaxation process for solution cast films at different temperatures. In the explored temperature region, similar to figure 6, two distinct slopes (a) and (c) are observed. Slope (a) refers to the activation energy of $0.7 \pm 0.05 \times 10^3$ kJ mol^{-1} required for the detachment and diffusion of one chain stem of approximately 30 nm length, a value in accordance with the measured crystal thickness [7]. Slope (c) refers to the activation energy of $4.2 \pm 1.0 \times 10^3$ kJ mol^{-1}, a value comparable to that of the respective process in the nascent UHMW-PE. This large activation energy is again associated with the breakdown of the crystal lattice. The absence of the slope (b) in figure 7 suggests that within the temperature region of 128–130.5 °C melting in these solution cast films mainly occurs by removal of single chain stems from the crystal substrate.

The activation energies (represented by slopes (a) and (c)) of the disentangled nascent sample in figure 6 and the solution crystallized sample in figure 7 are similar. Since the crystal thicknesses of the disentangled nascent and the solution crystallized samples are comparable, and both samples can be deformed mechanically in the solid state, this suggests that the activation energy required for the respective processes, namely the removal of single chain stems from the surface followed by their diffusion in the melt (slope (a)), as well as the breakdown of larger parts of the crystal lattice (slope (c)), occurs independent of the differences

[6] Considering one-third fewer neighbour interactions on the surface than in bulk, the detachment energy and its diffusion into the melt is likely to be 2.7 kJ mol^{-1} since the melting enthalpy of the bulk is 4.11 kJ mol^{-1} CH_2, a value obtained from the ATHAS data bank (http://web.utk.edu/~athas/databank/welcome-db.html).

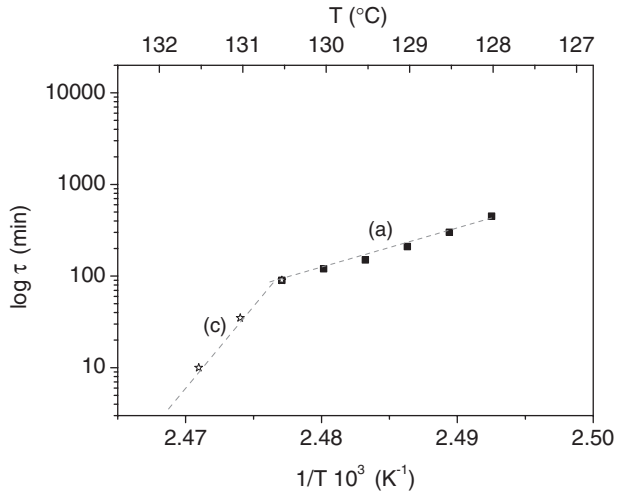

Figure 7. Arrhenius plot for solution crystallized UHMW-PE samples. The different relaxation times at the given annealing temperatures (determined from figure 5(d)) show two activated processes.

in the crystallization conditions of the two samples. The melting processes shown above are distinctly different from the melting behaviour observed for the melt crystallized samples, where only one melting process occurs at 135 °C (at a heating rate of 10 °C min^{-1}) without any time dependence of melting at low heating rates or at annealing temperatures below 135 °C. To follow reorganization in the crystal lattice prior to melting temperature modulated DSC (TM-DSC) on the entangled and disentangled nascent UHMW-PE is performed.

3.3. Reorganization in solid state prior to melting as probed by temperature modulated DSC (TM-DSC)

From the above described experiments it is evident that different processes are involved in the melting of crystals. Temperature modulated differential scanning calorimetric (TM-DSC) investigations provide the opportunity to separately measure the individual contributions of different processes to the TM-DSC apparent heat capacity signal. In the quasi-isothermal operation mode it is possible to study the contributions of time dependent processes occurring inside the sample upon small temperature fluctuations. Detailed information about such processes and the TM-DSC method can be found in a review article of Wunderlich [19]. Recently, Höhne *et al* reported a study on the pre-melting behaviour of entangled nascent UHMW-PE [20]. It was shown that with TM-DSC it is possible to determine the time constants of thermal activated processes, such as α-relaxation and reorganization processes, taking place within the crystal lattice.

By use of TM-DSC Höhne *et al* showed that the magnitude of the complex apparent heat capacity of the nascent entangled UHMW-PE in the pre-melting region is higher than the heat capacity obtained by conventional DSC in that region. This indicates that chain reorganization occurs in the solid state, which contributes to the apparent heat capacity. The magnitude of this 'excess heat capacity' decreases on second heating, suggesting that the process is irreversible in nature and is observed only on the first heating of the nascent sample. Quasi-isothermal TM-DSC experiments revealed that this apparent heat capacity is time dependent. To evaluate the relaxation times of the processes contributing to the apparent heat capacities requires the

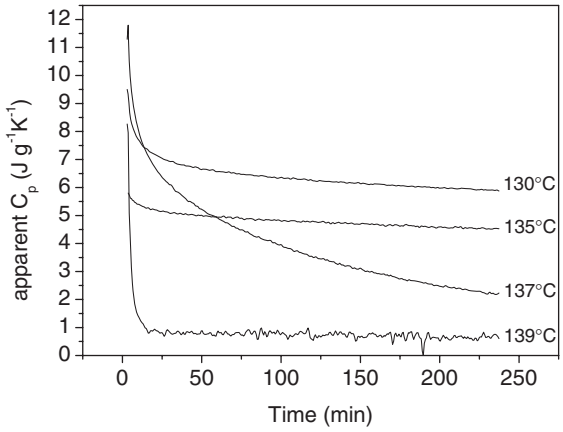

Figure 8. Apparent heat capacity from four quasi-isothermal TM-DSC measurements in the melting region of the disentangled nascent UHMW-PE (frequency 12.5 mHz, period 80 s, $T_A = 53$ mK).

assumption that the relaxation processes are of Arrhenius type (i.e. follow an exponential decay). With such an assumption an evaluation of the measured apparent heat capacity signals is possible, but it should be mentioned that due to the large uncertainty of the determined relaxation times the results are not clear and an interpretation may be difficult.

However, the method for the nascent entangled sample, described in [20], is also used for the determination of different relaxation times in nascent disentangled UHMW-PE. Quasi-isothermal TM-DSC measurements with the disentangled nascent UHMW-PE samples are performed at different temperatures below the melting peak and the change of the apparent heat capacity in time is followed (figure 8).

The respective excess heat capacity function is fitted with a sum of two or three exponentials $a_1 e_1^{-t/\tau} + a_2 e_2^{-t/\tau} (+a_3 e_3^{-t/\tau})$ and the result of the best fit, within the experimental accuracy, is plotted in figure 8. The approximately linear behaviour in this so-called Arrhenius-plot supports the assumption that the respective processes are of Arrhenius type (equation (2)). Therefore, the activation energies can be determined from the slopes in figure 9. Thus determined activation energies for reorganization in the solid state are 30 ± 10, 60 ± 10 and 500 ± 150 kJ mol^{-1}, respectively, for the three processes found in this sample. The first process (shown by solid symbols along line (a) in figure 9) is exothermic and can be attributed to ordering and perfection of the crystals. The activation energy of process (a) is of the same order of magnitude as the activation energy of the α-process (i.e. the chain diffusion within the crystallites) determined from mechanical measurements [21]. The second process (shown by the unfilled symbols along line (b) in figure 9) is endothermic and can be attributed to irreversible crystal thickening (and/or melting of small crystallites), processes well known in the literature [20–22]. These two processes start already at approximately 100 °C, well below the onset of the melting temperature, therefore these processes are attributed to reorganization in the solid state. Considering the small activation energy (30 ± 10, 60 ± 10 kJ mol^{-1}), such a process is likely to involve a few methylene units.

The third process, observed above 130 °C in the TM-DSC experiments (unfilled symbols along line (c) in figure 9), is linked to the irreversible melting. It seems to be one of the melting processes seen by the conventional DSC studies mentioned in the section above. To show the similarity, the data points obtained from the slope (a) of figure 6 are inserted as star symbols (*) in figure 9. Both data sets coincide, indicating the two relaxation processes to be

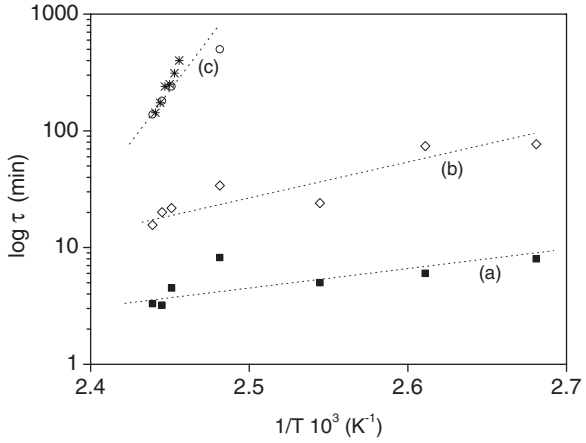

Figure 9. Activation diagram of the three processes determined from figure 8. The slope gives the activation energy (solid symbols, exothermic; open symbols, endothermic). The stars represent the time constants determined from the slope (a) of figure 6. This is attributed to the melting and diffusion of the stems from the crystal sides. The activation energy is determined from the slopes.

of similar origin. Considering the similar relaxation times and activation energies for line (c) in figure 9 and line (a) in figure 6, we attribute the third process from the TM-DSC experiments to the detachment of one chain stem from the crystal substrate and its diffusion to the melt. Considering the results from TM-DSC and annealing experiments with conventional DSC in good agreement, the assumptions made for the evaluation of the TM-DSC should be valid. Thus the processes seem to be of Arrhenius type and their characterization with the given parameters to be realistic.

3.4. Origin of the first high melting point of nascent and solution crystallized UHMW-PE

If we compare the low activation energy of 30 and 60 kJ mol^{-1} for the first and second processes of the TM-DSC evaluation with the activation energy required for the detachment of a chain stem ($\sim$600 kJ mol^{-1}), it is concluded that both the crystal perfection (first process) and the thickening (second process) takes place with the involvement of a few methylene units within the crystal. The reorganization occurs without any detachment of a whole chain stem. The third process takes place when the disentangled polymer sample is annealed close to the onset melting temperature; in this case, melting proceeds by successive detachment of chain stems from the crystal substrate and diffusion into the neighbouring melt. The minimum temperature required for this process is in good agreement with the melting temperature determined from the Gibbs–Thomson equation. At higher annealing temperatures ($>135.5\,^{\circ}C$) another melting process occurs where bigger clusters, exceeding the size of one stem, are co-operatively involved.

The relaxation times required for the successive detachment of chain stems from crystal substrate (>150 min) are considerably longer than the relaxation times for melting in clusters. Apparently, at standard heating rates, melting mainly proceeds via the cluster melting, involving seven or eight chain stems. The experiments show clearly that such a cluster melting of the nascent UHMW-PE always leads to a high melting temperature of 141 °C, normally representative of extended chain crystals only. In the second heating of the nascent samples (i.e. melt crystallized), no time dependent melting on annealing is observed and the normal melting temperature is 5 °C lower than the melting temperature of the nascent polymer during

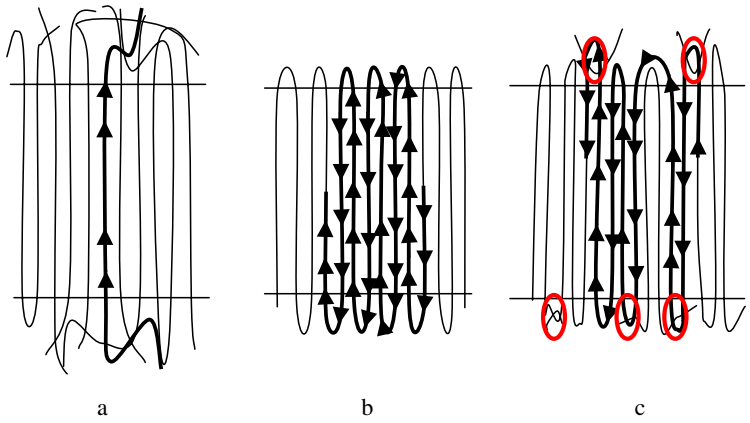

Figure 10. Illustration of the crystal structure of (a) melt-crystallized sample having inter crystal molecules and loose loops, (b) nascent disentangled sample having tight folds and (c) nascent entangled sample having tight folds. The depicted entanglements in the figure are circled.

the first run. These findings suggest that the above described cluster melting is absent in the melt crystallized samples. From this it is concluded that distinction in the melting behaviour and temperature depends on the topological differences of the chains in the amorphous region of the semi-crystalline polymers rather than on the crystal size.

Topological differences in the amorphous phase will arise from the nature of chain folding on the crystal surface, i.e. tight or loose folds [23]. In general, crystal melting is described by increasing the number of defects in the crystal lattice, ultimately leading to complete breakdown of the lattice. In semi-crystalline polymers where a chain within the lattice is connected by the chain segments in the amorphous phase, melting requires cooperative motion of the chain segments within the lattice and in the amorphous phase. Tight or loose chain folds connecting chains in the amorphous and crystalline regions will have implications in the breakdown of the crystal lattice. This concept is shown schematically in figure 10. In the case of nascent UHMW-PE with adjacent or tight folds, a greater number of $–CH_2–$ groups have to move cooperatively (figures 10(b) and (c)), thus the melting process, where the whole chain has to acquire a random coil state, requires the number of $–CH_2–$ groups to be higher than those present in a single chain stem residing within the crystal lattice. This cooperative melting will involve several chain stems connected by tight folds, thus higher melting temperature than that predicted from the Gibbs–Thomson equation.

In the melt crystallized UHMW-PE sample chain segments in the amorphous phase are free to adopt larger numbers of chain conformations, thus the crystal stems are connected by loose folds. Thus melting requires an entropy gain of the chain stem corresponding to crystal thickness (shown schematically in figure 10(a)). Therefore the number of repeating units involved in the melting process corresponds to the lamella thickness of the crystal, resulting in a melting point of 135 °C, as predicted from the Gibbs–Thomson equation.

By modifying the Gibbs–Thomson equation, Höhne [14, 18] correlated the number of CH_2 units with the melting temperature. In this approach the number of $–CH_2–$ groups of the respective molecule, incorporated into the crystallite via tight folds (methylene units present in the amorphous phase having restricted chain conformation [23]) is the essential variable, rather than the crystal thickness. In this approach the basic idea is that the total (molar) enthalpy $\Delta_m H_{\mathrm{mol}}$ and entropy $\Delta_m S_{\mathrm{mol}}$ of fusion (melting) of chain molecules each consisting of n repeating units in the crystals is composed of the respective values of the subunits.

The modified Gibbs–Thomson equation replaces crystal thickness by the number of repeating units,

$$\frac{1}{T_m^n} \approx \frac{1}{T_m^\infty}\left(1 - \frac{\Delta_m G_e}{\Delta_m H_{r.u.}^\infty}\frac{1}{n}\right) \tag{3}$$

which contains the number n of repeating units of the chain molecule (–CH_2– in UHMW-PE) rather than the crystal thickness and a quantity which is the total excess (Gibbs) free energy rather than only the surface free energy. Usually the number n of repeating units of the chain is unambiguously connected with the thickness of the respective lamella crystal via the well defined distance between two repeating units in the chain and possible tilt angle of the chain inside the crystal. In the case of cluster melting of seven or eight stems, from the number of CH_2 units ($\pm$1800) involved in the melting process a melting temperature of 138.5 °C is predicted by using equation (3). This value is in agreement with the experimentally determined melting temperature (138.2 °C) obtained on extrapolation to zero heating rate (figure 2).

From the thermal analysis studies it is apparent that melting temperature and melting process strongly depend on the topological constraints present in the amorphous region of the semi-crystalline polymer. Figure 6 clearly shows two distinct melting regions, i.e. slow melting ranging from 133.5 to 135.5 °C and fast melting ranging from 136 to 141 °C. To probe the structural changes during the melting processes in the fast and slow melting regions solid-state NMR studies are performed.

3.5. Melting in UHMW-PE probed by solid-state NMR

Polymer ^{1}H NMR lineshapes and spin–spin (T_2) relaxation are strongly affected by rotational chain motions at timescales $< 10^{-3}$ s. The more restricted the motion, the broader is the resonance and the faster the relaxation decay of the so-called Hahn-echo produced by a 90°-τ-180°-τ pulse sequence versus the echo time 2τ. Spin–spin relaxation is a better measure for polymer chain motion than the lineshape, because the latter is also broadened by other mechanisms, which are eliminated in the Hahn-echo experiment. ^{1}H NMR T_2 relaxometry is therefore a regular tool to determine entanglement and cross-link density in rubbers [24–27] and polymer melts [28, 29]. At $T \gg T_g$ chain mobility at timescales $< 10^{-3}$ s is controlled by chemical cross-links and physical entanglements with lifetimes $> 10^{-3}$ s. The underlying assumption is that polymer motions are divided into fast and slow polymer motions at the 10^{-3} s timescale without significant intermediate fraction. To distinguish between the crystalline and amorphous phases of entangled and disentangled nascent UHMW-PE, the relatively robust and quantitative Hahn-echo method is applied as a tool.

^{1}H NMR Hahn echo decays are monitored at a constant temperature (figures 11 and 12). Between the experiments at different temperatures, the sample is heated at a rate of 0.1 °C min^{-1}. Below the onset of melting temperature the observed Hahn-echo decays of the nascent entangled UHMW-PE sample are well described in terms of two exponential components (figure 11). The fastest component has a fairly temperature-independent short T_2 value ~10 μs and disappears above 140 °C. This fast relaxation time is assigned to the rigid, crystalline phase. Above 120 °C, the long T_2 relaxation time of the amorphous fraction increases strongly with temperature. The steepest increase occurs around the melting point $T_m \sim 140$ °C. Apparently, below T_m chain motion in the entangled amorphous phase is confined by the crystalline domains. The resulting melt state is described by a single T_2 relaxation time of ~1 ms.

Using a similar heating protocol a third T_2 component seems to show up in the Hahn-echo decays of the nascent disentangled sample (figure 12). This component appears in addition to

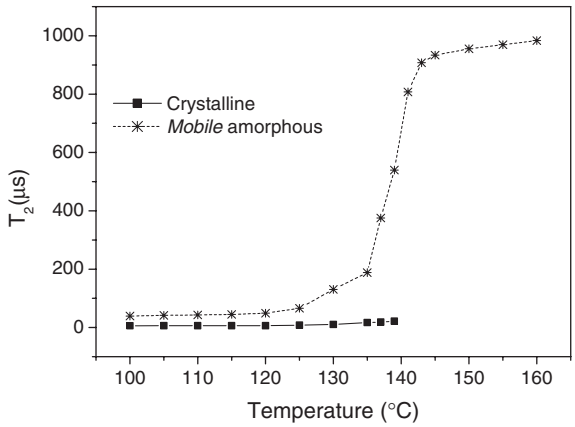

Figure 11. T_2 relaxation time versus temperature of nascent entangled UHMW-PE (reproduced from [32]).

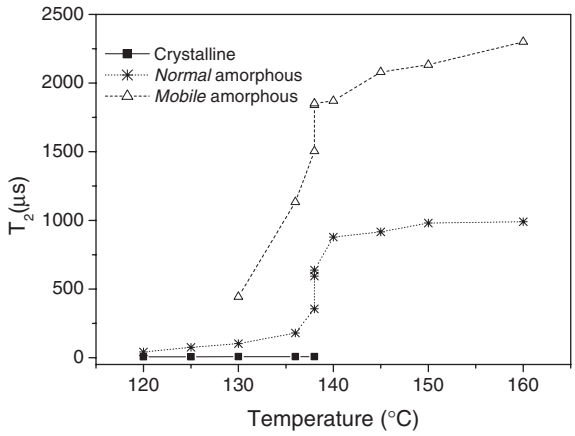

Figure 12. T_2 relaxation time versus temperature of the nascent disentangled UHMW-PE (reproduced from [32]).

the crystalline and amorphous T_2 components also found for the nascent entangled UHMW-PE. The short T_2 attributed to the crystalline phase and the long T_2 attributed to the amorphous phase of the disentangled nascent sample are similar to T_2 relaxation times determined for the crystalline and the amorphous phases of the nascent entangled sample. The value of this third T_2 component is about two to three times longer than that of the amorphous phase. Because of its long T_2 value, we attribute the third T_2 component to a more *mobile* type of amorphous phase, to be distinguished from the *normal* amorphous phase observed for the entangled and disentangled nascent UHMW-PE.

Quantitative determination of the nascent disentangled sample is shown in figure 13. The crystalline fraction (shortest T_2 component) of approximately 72% determined from the Hahn-echo decay at 120 °C is consistent with the crystallinity of the sample estimated from DSC. As the crystallinity decreases with increasing temperature from 130 to 137 °C, the *normal* amorphous fraction increases (figure 13). Upon further increasing the temperature above

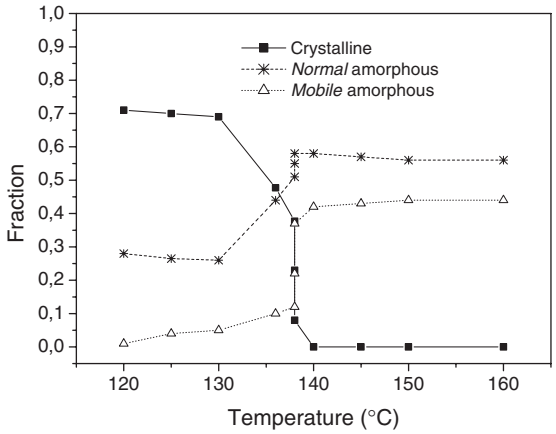

Figure 13. Changes in the relative fractions of the crystalline, mobile amorphous and normal amorphous components of the disentangled nascent UHMW-PE sample with temperature as probed from a Hahn echo pulse program (reproduced from [32]).

137 °C, with the disappearance of the crystalline phase, the highly mobile amorphous phase increases simultaneously.

To recall, melting at the low temperatures (with 0.1 °C min^{-1} from 130 to 137 °C) is associated with the successive detachment and diffusion of a few crystal stems from the crystal surface (figure 6). The increase of the normal amorphous fraction suggests that the polymer chain stems that are molten by the successive detachment are able to entangle with the surrounding amorphous phase. Upon increasing the temperature further with the melting of the remainder of the disentangled crystalline fraction (approximately 40%) a highly *mobile* amorphous component, of the same fraction, evolves. The amount of the highly *mobile* amorphous fraction as well as the *normal* amorphous fraction remains almost constant upon further increasing temperature. This suggests a barrier for the mixing of the two amorphous phases. As the polyethylene chains are chemically uniform, the presence of the two amorphous fractions with two different mobilities above 140 °C originates from the 'heterogeneous' distribution of entanglements, which arises on slow melting of the disentangled crystals.

On *fast* heating (10 °C min^{-1}) of the disentangled nascent sample to its melt state, the T_2 relaxation time determined at 150 °C is faster than the T_2 relaxation time determined at 150 °C in the *slowly* heated sample (0.1 °C min^{-1}) to its melt state; see figure 14(a). In contrast to the *slowly* heated sample, in the *fast* heated sample the *mobile* amorphous component is absent and the T_2 relaxation can be described with a single relaxation time. The T_2 relaxation at 150 °C determined for the entangled nascent sample, shown in figure 14(b), is independent of heating rate. Using the different T_2 relaxation time as a filter, thereby suppressing the less mobile fractions of the melt, we observe significant differences in the peak width of the NMR spectrum of the two melt states arising with different heating rates from the initially disentangled nascent sample. The narrower peak of the slowly heated melt indicates a higher local mobility in part of the sample, whereas the T_2-filtered peak width of the initially entangled sample is independent of the heating rate (figure 14(b)). The observed peak width is similar to the fast heated disentangled melt (figure 14(a)). In fact, an increase in T_2 filter time leads to suppression of the rigid fractions of the sample and decreasing peak width in the slow heated disentangled melts, strengthening the idea of heterogeneity in the local mobility.

These dynamic NMR results suggest that upon fast melting, associated with melting in clusters of seven or eight polymer chain stems, the chains are homogenously distributed in

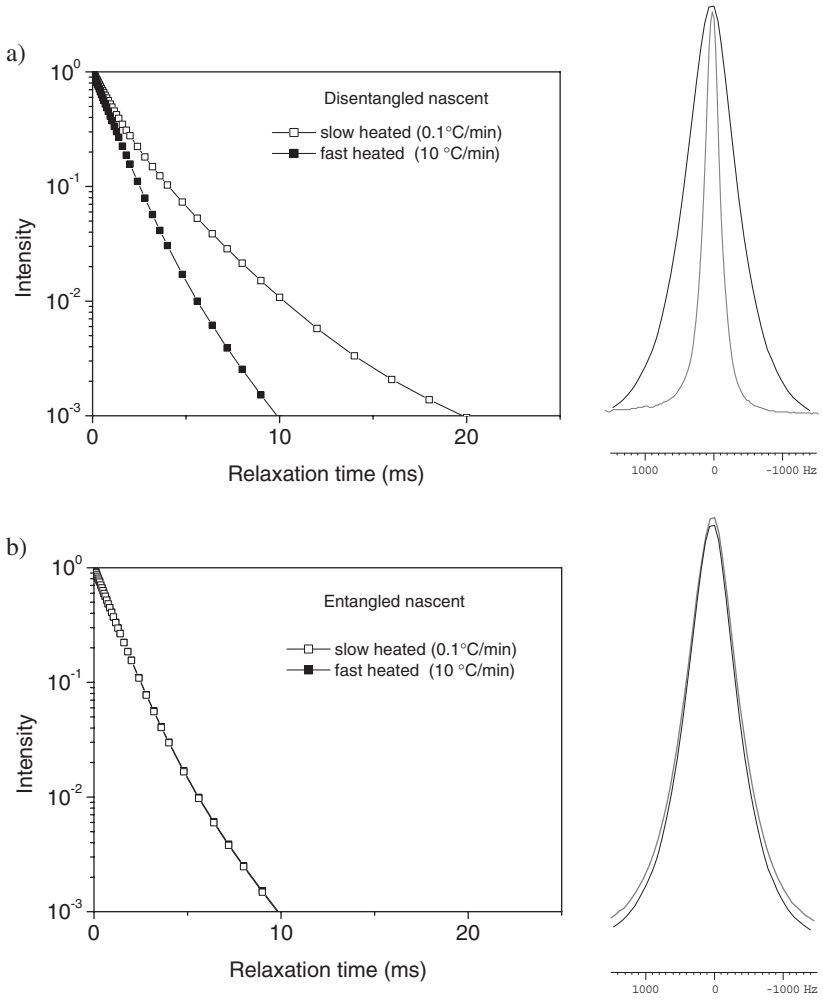

Figure 14. NMR line shapes and T_2 relaxation curves of fast (10 °C min^{-1}, filled squares) and slow (0.1 °C min^{-1}, unfilled squares) heated UHMW-PE melts of the initially entangled and disentangled nascent samples. Experiments are performed at 150 °C. The dynamic heterogeneity of the slow heated disentangled nascent sample can be monitored as well via variation of the line width in the T_2-filtered spectra (10 ms is the applied T_2 relaxation filter time) (reproduced from [32]).

the melt, resulting in a homogenous distribution of entanglements. If the disentangled nascent UHMW-PE is given more time to melt (slow heating), the crystals are molten first from the sides (chain ends) before complete breakdown of the crystal lattice occurs. The resulting melt state contains a heterogeneous distribution of chain entanglements. The resulting melt state exhibits interesting rheological phenomena as summarized in [3].

3.6. Melt mechanism

Combining the results from DSC and solid-state NMR a hypothesis for the melt mechanism involved in melting of the disentangled nascent UHMW-PE can be proposed. Figure 15 depicts slow melting of the disentangled nascent crystals. The adjacently re-entrant chains melt by

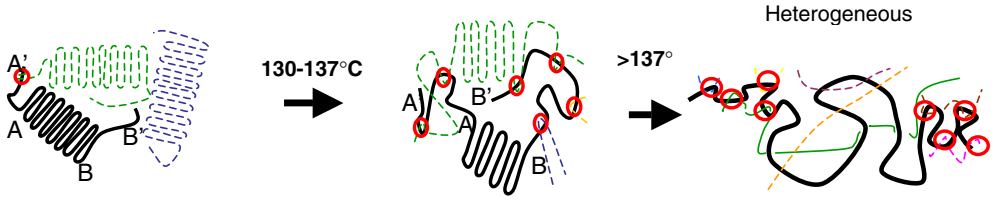

Figure 15. Depicting melting process of the disentangled nascent crystals during slow heating. On annealing below 137 °C, with the consecutive detachment of chain stems from the crystal substrate and their diffusion in the melt, the normal entangled amorphous phase is formed. On heating above 137 °C the remainder of the crystal melts, invoking the mobile amorphous phase. The two amorphous phases, mobile and normal, do not mix even above the melting temperature. This leads to the origin of a melt having differences in the local mobility of the two amorphous components. Entanglements are encircled (reproduced from [3]).

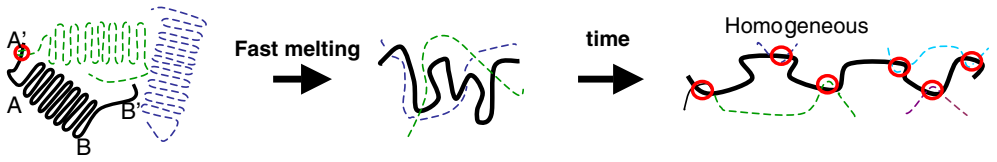

Figure 16. The melting process of the disentangled nascent crystals during fast heating (reproduced from [3]).

consecutive detachment of a chain segments equal to the crystal thickness (from the crystal sides) from the crystal lattice (AA′ and BB′ in figure 15). The initially disentangled chains will form entanglements by reptation (circles) and will result in a low T_2 relaxation time. Upon melting the whole crystal at higher temperatures, the section AB in figure 15 will transform from a disentangled crystal to a disentangled amorphous phase (as was shown in the NMR experiments). As a result of the absence of physical entanglements, the disentangled component of the amorphous fraction can be described by a high T_2 value referring to the overall higher local mobility. Thus, depending on the heating rate, chain dynamics in the resultant melt state of the disentangled nascent crystals can be altered. A detailed study on the influence of heating rate on chain dynamics is reported elsewhere [4, 23].

In contrast to the slow melting, a complete collapse of the crystal lattice occurs upon fast melting. This causes an instant free movement of the chain ends in the melt, resulting in a homogenous distribution of entanglements (figure 16).

In the nascent entangled samples, physical entanglements present in the amorphous phase of the semi-crystalline polymer restrict the consecutive detachment of chains. Therefore, the low activation energy component (a) in figure 6 is absent. Thus on melting, independent of the heating rate, entanglements present in the amorphous phase are homogeneously distributed along the main chain (figure 17).

3.7. Melting kinetics in UHMW-PE probed by rheology

Differences in the melting process of the entangled and disentangled nascent polymers can be also depicted from rheological studies. The entangled and disentangled samples are kept at a constant annealing temperature of 134 °C. The elastic modulus is followed as a function of time at a constant strain of 0.5% (inside the viscous–elastic linear regime) and frequency 10 rad s^{-1} (inside the rubbery plateau modulus time frame). On annealing the disentangled and entangled

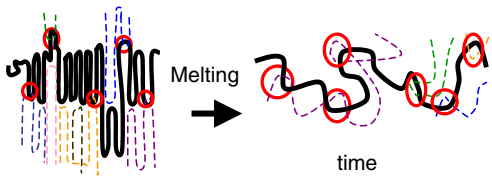

Figure 17. Depicting the melting process of the entangled nascent crystals. On melting, entanglements initially present in the amorphous phase are homogeneously distributed (reproduced from [3]).

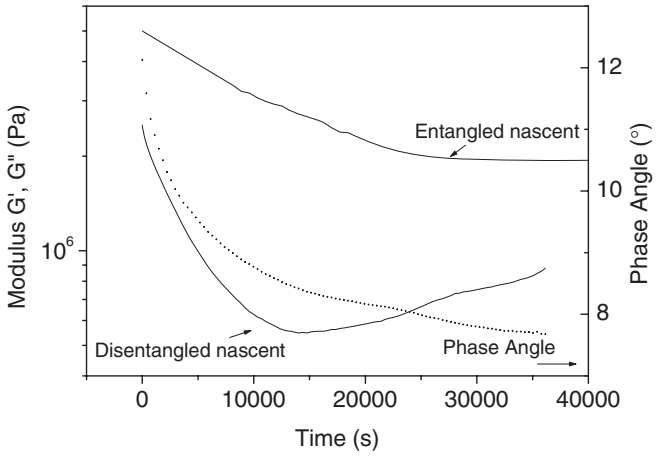

Figure 18. Elastic modulus of the entangled and disentangled nascent UHMW-PE as a function of time at a fixed frequency of 10 rad s^{-1}, strain (0.5%) and temperature 134 °C. The phase angle plotted in the figure is from the annealing experiment of the disentangled sample.

nascent samples the phase angle decreases with time following a first order exponential decay (figure 18). This decrease in phase angle and the modulus is attributed to melting of the crystals. Similar to the findings presented above, the melting is characterized by a single relaxation time. Distinction in the modulus of the entangled and disentangled polymers is evident. On melting of the entangled nascent sample, the elastic modulus decreases to 2 MPa, corresponding to the plateau modulus of the fully entangled melt state, whereas the disentangled sample shows an initial drop in the modulus to 0.6 MPa followed by an increase with time. These rheological differences originating from the melting behaviour of the entangled and disentangled nascent UHMW-PE are in agreement with the differences observed in the same samples studied by solid-state NMR. To recall, on melting of the entangled nascent sample a *normal* melt state arises, which is entangled.

On the other hand, on slow melting of the disentangled nascent sample a *mobile* melt state together with a normal melt state is realized. The presence of this mobile melt state causes a lower plateau modulus than that anticipated from the normal melt state. Hence we can designate the origin of the *mobile* component in the melt to be disentangled. In figure 18 the increase in plateau modulus of the disentangled nascent polymer after 15 000 s is a result of entanglement formation.

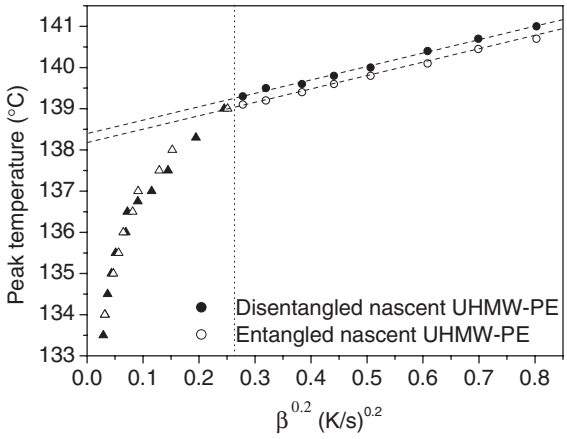

Figure 19. The measured melting peak temperatures for the entangled and the disentangled nascent UHMW-PE at different heating rates. The non-linear abscissa allows extrapolation to zero heating rate [15]. However, the extrapolation fails at the lower heating rates.

4. Conclusions

From the series of experiments reported above it is evident that melting of the nascent, solution crystallized and melt crystallized UHMW-PE samples shows differences in melting processes. The number of CH_2-groups that are involved in a melt process depends on the temperature as well as on the time scale. Melting in the low temperature region (130–135 °C) occurs by cooperative detachment of chain stems from the surface involving a time dependent melting process, whereas melting in the high temperature region (136–141 °C) leads to a breakdown of larger parts of the lattice. Therefore the normal extrapolation to zero heating rate of figure 2 needs modification at slow heating rates, as shown in figure 19. The figure shows that in nascent polymers, if melting kinetics is taken into account, the normal extrapolation to zero heating rate does not hold good.

The high melting temperature of nascent and solution crystallized UHMW-PE compared to that of melt crystallized UHMW-PE is explained by the differences in the crystal topology; i.e., depending on the nature of chain folds in the crystal, loose or tight, the number of CH_2 units that require cooperative motion for melting differs. A melt crystallized sample, having loose folds, melts at the temperature predicted by the Gibbs–Thomson equation; i.e., the number of CH_2 units that require cooperative motion to adopt the random coil state is equal to the crystal thickness. In nascent and solution crystallized samples, having tight folds, the number of CH_2 units required for cooperative melting is much larger than that of the crystal thickness. Therefore, the melting point of the samples shifts to higher temperatures than the melt-crystallized sample.

From the structural information probed by solid-state ^{1}H NMR, the influence of the different melting processes on the local mobility of the amorphous state is shown. The chain ends of the disentangled nascent sample which gets detached from the crystal sides prior to the melting (<135 °C) form entangled amorphous domains. Melting of the remainder of the crystal occurs at a higher temperature, leading to the origin of a melt with *mobile* disentangled and *normal* entangled amorphous domains. With the help of solid-state ^{1}H NMR, remarkable distinction in the distribution of the topological constraints in the melt can be probed. The disentangled melt state shows consistency with the origin of the lower plateau modulus determined by rheological studies.

A theory on the evolution of the heterogeneous melt state arising from the controlled melting of the disentangled crystals is proposed by McLeish [30]. The influence of the *mobile* disentangled domains on crystallization kinetics is addressed in [32]. The molar mass dependence on build-up of the modulus on melting of the disentangled samples as a function of time is addressed in [31]. Details of the work can be found in the PhD thesis [33].

Acknowledgments

The authors wish to acknowledge constructive discussions with Professor Hans W Spiess and Dr Robert Graf of the Max Planck Institute for Polymers in Mainz, Germany.

References

[1] Smith P, Chanzy H D and Rotzinger B P 1985 *Polym. Commun.* **26** 258
[2] Rotzinger B P, Chanzy H D and Smith P 1989 *Polymer* **30** 1814
[3] Rastogi S, Lippits D R, Peters G W M, Graf R, Yao Y and Spiess H W 2005 *Nat. Mater.* **4** 635
[4] Lemstra P J, Bastiaansen C W M and Rastogi S 2000 *Structure Formation in Polymeric Fibers* ed D R Salem (Munich: Hanser) chapter 5 ISBN 1-56990-306-9
[5] Tervoort-Engelen Y M T and Lemstra P J 1991 *Polym. Commun.* **32** 343
[6] Rastogi S, Kurelec L, Lippits D, Cuijpers J, Wimmer M and Lemstra P J 2005 *Biomacromolecules* **6** 942
[7] Corbeij-Kurelec L 2001 *PhD Thesis* Eindhoven University of Technology, Chain mobility in polymer systems chapter 3 ISBN 90-386-3032-8 http://alexandria.tue.nl/extra2/200113706.pdf
[8] Wunderlich B and Czornyj G 1977 *Macromolecules* **10** 906
[9] Cho T Y, Heck B and Strobl G 2004 *Colloid Polym. Sci.* **282** 825
[10] Rastogi S, Spoelstra A B, Goossens J G P and Lemstra P J 1997 *Macromolecules* **30** 7880
[11] Lippits D R, Rastogi S and Höhne G W M 2006 *Phys. Rev. Lett.* **96** 218303
[12] Höhne G W H, Kurelec L, Rastogi S and Lemstra P J 2003 *Thermochim. Acta* **396** 97
[13] Höhne G W H 1997 *Thermochim. Acta* **304/305** 209
[14] Höhne G W H 2002 *Polymer* **43** 4689
[15] Toda A, Hikosaka M and Yamada K 2002 *Polymer* **43** 1667
[16] Cho T Y, Heck B and Strobl G 2004 *Colloid Polym. Sci.* **282** 825
[17] Atkins P W *Physical Chemistry* (Oxford: Oxford University Press) Chapter 24.6, 27,4, 28,12 ISBN 0199271836
[18] Höhne G W H 2003 *Thermochim. Acta* **403** 25
[19] Wunderlich B 2002 *Prog. Polym. Sci.* **391** 51
[20] Höhne G W H, Kurelec L, Rastogi S and Lemstra P J 2003 *Thermochim. Acta* **396** 97
[21] Mayr P U 1998 *Dissertation* Universität Ulm
[22] Wunderlich B 1980 *Macromolecular Physics* vol 3 *Crystal Melting* (New York: Academic)
[23] Yao Y, Graf R, Rastogi S and Spiess H W 2004 *IUPAC Macro 2004 (Paris)*
[24] Fry C G and Lind A C 1988 *Macromolecules* **21** 1292
[25] Wouters M E L, Litvinov V M, Binsbergen F L, Goossens J G P, van Duin M and Dikland H G 2003 *Macromolecules* **36** 1147
[26] Tillier D L, Meuldijk J, Magusin P C M M, van Herk A M and Koning C E 2005 *J. Polym. Sci.* A **43** 3600
[27] Orza R A, Magusin P C M M, Litvinov V M, van Duin M and Michels M A 2005 *Macromol. Symp.* **230** 144
[28] Cosgrove T, Turner M J, Griffiths P C, Hollingshurst J, Shenton M J and Semlyen J A 1996 *Polymer* **37** 1535
[29] Guillermo A, Cohen Addad J P and Bytchenkoff D 2000 *J. Chem. Phys.* **113** 5098
[30] McLeish T C B 2007 *Soft Matter* **3** 83
[31] Lippits D R, Rastogi S, Talebi S and Bailly C 2006 *Macromolecules* **39** 8882
[32] Lippits D R, Rastogi S, Höhne G W M, Mezari B and Magusin P C M M 2007 *Macromolecules* at press http://pubs.acs.org/cgi-bin/asap.cgi/mamobx/asap/pdf/ma0622837.pdf
[33] Lippits D R 2007 Heterogeneity in polymer melts by controlled melting of polymer crystals *PhD Thesis* Eindhoven University of Technology